

# Extended Perturbation Theory for the Local Density Distribution Function

S. Colombi<sup>1,3</sup>, F. Bernardeau<sup>2</sup>, F.R. Bouchet<sup>3</sup>, and L. Hernquist<sup>4,5</sup>

<sup>1</sup> *CITA, 60 St George St., Toronto, ON M5S 3H8, Canada*

<sup>2</sup> *Service de Physique Théorique, C.E. de Saclay, F-91191 Gif-sur-Yvette cédex, France*

<sup>3</sup> *Institut d'Astrophysique de Paris, 98 bis boulevard Arago, F-75014 Paris, France*

<sup>4</sup> *Board of Studies in Astronomy and Astrophysics, University of California, Santa Cruz, CA 95064, U.S.A.*

<sup>5</sup> *Presidential Faculty Fellow*

## ABSTRACT

Perturbation theory makes it possible to calculate the probability distribution function (PDF) of the large scale density field in the small variance limit,  $\sigma \ll 1$ . For top hat smoothing and scale-free Gaussian initial fluctuations, the result depends only on the linear variance,  $\sigma_{\text{linear}}$ , and its logarithmic derivative with respect to the filtering scale  $-(n_{\text{linear}} + 3) = d \log \sigma_{\text{linear}}^2 / d \log \ell$  (Bernardeau 1994a).

In this paper, we measure the PDF and its low-order moments in scale-free simulations evolved well into the nonlinear regime and compare the results with the above predictions, assuming that the spectral index and the variance are *adjustable* parameters,  $n_{\text{eff}}$  and  $\sigma_{\text{eff}} \equiv \sigma$ , where  $\sigma$  is the true, nonlinear variance. With these additional degrees of freedom, results from perturbation theory provide a good fit of the PDFs, even in the highly nonlinear regime. The value of  $n_{\text{eff}}$  is of course equal to  $n_{\text{linear}}$  when  $\sigma \ll 1$ , and it decreases with increasing  $\sigma$ . A nearly flat plateau is reached when  $\sigma \gg 1$ . In this regime, the difference between  $n_{\text{eff}}$  and  $n_{\text{linear}}$  increases when  $n_{\text{linear}}$  decreases. For initial power-spectra with  $n_{\text{linear}} = -2, -1, 0, +1$ , we find  $n_{\text{eff}} \simeq -9, -3, -1, -0.5$  when  $\sigma^2 \simeq 100$ .

It is worth noting that  $-(3+n_{\text{eff}})$  is *different* from the logarithmic derivative of the nonlinear variance with respect to the filtering scale. Consequently, it is not straightforward to determine the nonlinearly evolved PDF from arbitrary (scale-dependent) initial conditions, such as Cold Dark Matter, although we propose a simple method that makes this feasible.

Thus, estimates of the variance (using, for example, the prescription proposed by Hamilton et al. 1991) and of  $n_{\text{eff}}$  as functions of scale for a given power spectrum makes it possible to calculate the local density PDF at any time from the initial conditions.

**Key words:** cosmology: theory – galaxies: clustering – methods: numerical – methods: statistical

## 1 INTRODUCTION

It is generally believed that the large-scale structures of the Universe, such as those seen in the distribution of galaxies, arose through gravitational instability from primordial seed fluctuations. On scales larger than roughly  $8 h^{-1} \text{Mpc}^*$ , the dynamics of the Universe is dominated by gravitational forces, implying that the matter behaves as if it were purely nonbaryonic and collision-less. Thus, when curvature can be neglected (for scales below  $500 h^{-1} \text{Mpc}$ ), the evolution of the Universe can be described by the Vlasov-Poisson sys-

tem of equations, in coordinates comoving with the cosmic expansion. In general, nonlinear coupling makes it virtually impossible to solve these equations analytically. Thus, on small scales, where density contrasts are large,  $N$ -body simulations are typically used to obtain numerical solutions. However, on scales larger than about  $10 h^{-1} \text{Mpc}$ , the amplitude of the density fluctuations is modest and *Perturbation Theory* (PT) can be used to compute statistical properties of the cosmic fields.

Here, we focus on the Probability Distribution Function (PDF) of the local density smoothed with a spherical filter of radius  $\ell$  at a time  $t$ ,  $P(\rho, \ell, t)$ . The PDF, a simple to measure statistic, has been widely used to characterize the statistical properties of the large scale galaxy distribution

\* We adopt  $h = H_0 / (100 \text{ km/s/Mpc})$ , where  $H_0$  is the Hubble constant.

(see, e.g., Alimi, Blanchard & Schaeffer 1990; Maurogordato, Schaeffer & da Costa 1992; Szapudi, Szalay & Boschán 1992; Bouchet et al. 1993; Gaztañaga 1992, 1994; Szapudi, Meiksin & Nichol 1996).

Our aim is to determine whether there is a simple relationship between the PDF obtained for the matter distribution in the nonlinear regime and the one predicted by PT. The latter should, in principle, be valid only in the weakly nonlinear regime. In our calculations, we assume i) that the Universe is flat with  $\Omega = 1$ , and ii) that the initial fluctuations of the density field were Gaussian, pressure-less (i.e. cold), and scale-free.

In real galaxy catalogs, the interpretation of the results is complicated by systematic effects, such as the so-called bias between the galaxy distribution and the matter distribution (e.g., Fry & Gaztañaga 1993, Juszkiewicz et al. 1995), redshift distortions in three-dimensional catalogs (e.g., Matsubara & Suto 1994; Hivon et al. 1995), and effects of projection along the line of sight in two-dimensional catalogs (e.g., Bernardeau 1995). In what follows, we focus on the statistical properties of the *matter* distribution and thus neglect these effects.

Let  $\sigma^2(\ell)$  be the variance of the PDF. In the weakly nonlinear regime ( $\sigma^2 \ll 1$ ) the scale-free nature of the initial conditions implies

$$\sigma^2 \approx \sigma_{\text{linear}}^2 \propto \ell^{-(n_{\text{linear}}+3)}. \quad (1)$$

In general, the PDF of the local density can be characterized by the behavior of its cumulants (i.e. the connected part of the moments),  $\langle \delta^q \rangle_c$  (see e.g. Bernardeau 1994a, hereafter B94 for a more precise definition). Note that  $\langle \delta^2 \rangle_c = \langle \delta^2 \rangle = \sigma^2(\ell)$ , where  $\delta$  is the density contrast  $\delta = \rho/\langle \rho \rangle - 1$ . When the variance is small, the dominant contribution to all the cumulants can be calculated analytically from PT for a top-hat smoothing window (B94). The result is that the quantities  $S_q$  defined by

$$S_q(\sigma) \equiv \frac{\langle \delta^q \rangle_c}{\sigma^{2(q-1)}}, \quad (2)$$

are all *finite constants* in the limit of small variance<sup>†</sup>. The next-to-leading order term is expected to be proportional to  $\sigma^2$ , so that

$$S_q(\sigma) = S_q^{\text{PT}} + \mathcal{O}(\sigma^2). \quad (3)$$

Comparisons with numerical simulations have shown that the PT predictions are accurate as long as  $\sigma < 1$  (Juszkiewicz et al. 1993, 1995; B94; Baugh, Gaztañaga & Efstathiou 1995; Gaztañaga & Baugh 1995; Lokas et al. 1995a,b). In this regime, the whole PDF can then be calculated analytically (B94), as a function of  $\ell$ ,  $\sigma_{\text{linear}}$  and  $n_{\text{linear}}$ :

$$P = P_{\text{PT}}(\rho, \sigma_{\text{linear}}, n_{\text{linear}}), \quad \sigma \ll 1. \quad (4)$$

It is important to notice that the measured cumulants in the observed galaxy distribution are also in good agreement with PT predictions in the weakly nonlinear regime (e.g.,

<sup>†</sup> Note that we have exploited the scale-free nature of the system to express the quantity  $S_q(\ell, t)$  as a function of only the variance. This would not be possible for scale dependent initial conditions such as Cold Dark Matter (CDM).

Bouchet et al. 1993, Gaztañaga 1994, Szapudi, Meiksin & Nichol 1996), given possible statistical uncertainties (e.g., Szapudi & Colombi 1996) and other systematic effects discussed earlier in this section.

For power-law spectra, the set of  $S_q^{\text{PT}}$  can be determined as a function of  $n_{\text{linear}}$  (Juszkiewicz & Bouchet 1992; Juszkiewicz, Bouchet & Colombi 1993; B94; Bernardeau 1994b):

$$S_3^{\text{PT}}(n_{\text{linear}}) = \frac{34}{7} - (n_{\text{linear}} + 3); \quad (5)$$

$$S_4^{\text{PT}}(n_{\text{linear}}) = \frac{60712}{1323} - \frac{62}{3}(n_{\text{linear}} + 3) + \frac{7}{3}(n_{\text{linear}} + 3)^2; \quad (6)$$

$$S_5^{\text{PT}}(n_{\text{linear}}) = \frac{200575880}{305613} - \frac{1847200}{3969}(n_{\text{linear}} + 3) + \frac{6940}{63}(n_{\text{linear}} + 3)^2 - \frac{235}{27}(n_{\text{linear}} + 3)^3, \quad (7)$$

and so on.

In what follows, we use these definitions as fitting functions of the  $S_q$  ratios, leaving  $n_{\text{linear}}$  as a free parameter. One can then invert the above equations to deduce, for each  $q$ , the value of  $n_{\text{linear}}$  which yields the measured value,  $S_q^{\text{meas}}$ , of the parameters  $S_q$ . We use this approach to define functions  $n_q(\sigma)$ , ( $q \geq 3$ ), by

$$S_q^{\text{PT}}[n_q(\sigma)] \equiv S_q^{\text{meas}}(\sigma). \quad (8)$$

Of course, as discussed above, the measured  $n_q$ 's are expected to have identical values in the weakly nonlinear regime ( $\sigma \ll 1$ ), and be equal to the value of the initial index  $n_{\text{linear}}$ .

In the nonlinear regime ( $\sigma \gtrsim 1$ ), however, results from perturbation theory are no longer valid, and we do not expect the functions  $n_q$  to take a universal (constant) value. Actually, there is no *a priori* reason why the relation  $n_q(\sigma) = n_{q'}(\sigma)$  should hold for  $q \neq q'$  and  $\sigma \gtrsim 1$ , even in the framework of the self-similar/stable clustering hypothesis, where the functions  $n_q(\sigma)$  are expected to approach constants in the highly nonlinear regime (e.g., Davis & Peebles 1977; Peebles 1980; Balian & Schaeffer 1989, hereafter BS).

In this paper, we use measurements of the PDF by Colombi, Bouchet & Hernquist (1996, hereafter CBH) in  $N$ -body simulations of flat universes with scale-free initial conditions to show that, within the accuracy of the calculations, all functions  $n_q$  superpose to give a unique function  $n_{\text{eff}}$

$$n_{\text{eff}}(\sigma) = n_q(\sigma). \quad (9)$$

The measurement of  $S_q$  is difficult when  $q$  is larger than a few, because of systematic errors due to finite volume effects (e.g., Colombi, Bouchet & Schaeffer 1994, 1995, hereafter CBSI and CBSII). However, one can check the validity of the property (9) from the overall *shape* of the PDF rather than with its moments. This would mean that PT can be applied to the nonlinear regime as follows:

$$P = P_{\text{PT}}[\rho, \sigma, n_{\text{eff}}(\sigma)]. \quad (10)$$

We shall refer to this generalization as *Extended Perturbation Theory* (EPT). The only quantities that would be needed to compute the PDF, if EPT applies, are the functions  $n_{\text{eff}}(\sigma)$  and the variance itself. If valid, EPT would thus result in tremendous simplification.

This paper is organized as follows. In Section 2, we present the measured quantities  $n_q$ ,  $3 \leq q \leq 5$  as functions of the variance in our  $N$ -body simulations and show that they indeed define a unique function  $n_{\text{eff}}(\sigma)$  that can be fitted analytically. We then compare the PDF predicted by EPT to that measured for different values of  $\sigma$ . The results allow an extrapolation to non power-law spectra. In section 3 we discuss the asymptotic behavior of the density PDFs in the EPT framework which depends only on a few parameters. We relate them to the  $n_{\text{eff}}$  found. We conclude in section 4 by summarizing our results and discuss them in light of related works. For completeness, in the appendix we summarize the results obtained from PT, the generic properties expected for the density PDF, and the algorithm used to compute it numerically.

## 2 MEASUREMENTS

The scale-free simulations we analyze are described in detail in CBH. They were performed with the cosmological tree-code of Hernquist, Bouchet & Suto (1991), using  $64^3$  particles and periodic boundaries. We consider four values of the spectral index:  $n_{\text{linear}} = -2, -1$  (two  $N$ -body sets), 0 and +1. CBH measured the count probability distribution function (CPDF)  $P_N(\ell)$  at various times in these simulations. The CPDF is just the probability of finding  $N$  particles in a spherical cell of radius  $\ell$  randomly thrown in the data set. Thus, the CPDF differs from the PDF: discreteness effects have to be accounted for to transform the CPDF into the PDF since the latter involves the underlying *continuous* density field. CBH computed the quantities  $S_q$ ,  $3 \leq q \leq 5$  from the moments of the CPDF, with the proper corrections for discreteness effects. They studied other contamination effects, such as artificial correlations related to the way initial conditions are generated, short range softening of the forces in the  $N$ -body simulations, and finite volume effects arising from missing waves longer than the box. In particular, CBH defined a reliable scale range over which finite volume corrections were applied. From these measurements of the functions  $S_q(\sigma)$ , we can directly infer  $n_q(\sigma)$  for  $3 \leq q \leq 5$ .

This section is organized as follows. First we study the functions  $n_q(\sigma)$  in § 2.1. We will see that they all superpose to a single function  $n_{\text{eff}}(\sigma)$  within the measurement errors. In § 2.2, we check whether this result applies to the CPDF itself, and in § 2.3, we present a possible extrapolation to non power-law spectra.

### 2.1 The effective spectral index $n_{\text{eff}}$

In Figure 1, we show the dependence of the deduced  $n_q$  on the variance, for each value of  $n_{\text{linear}}$ . The various symbols correspond to different values of  $q$ . They superpose, which is not surprising in the weakly nonlinear regime since all functions  $n_q$  should tend to the same value  $n_{\text{linear}}$  according to PT (although not perfectly; this point is discussed in detail by CBH). More interestingly, the superposition still

**Table 1.** Parameters used in fit I (eq. [11]).

$n_{\text{linear}}$	$n_{\text{nonlinear}}$	$n_{\text{nonlinear}}^-$	$n_{\text{nonlinear}}^+$	$\sigma_0$	$\tau$
-2	-9.5	-12.4	-7.22	1.6	1.4
-1	-3	-3.8	-2.24	1.4	1.2
0	-1.2	-1.6	-0.86	1.25	0.6
+1	-0.85	-1.17	-0.57	0.7	0.3

holds in the nonlinear regime where the vertical spread of the points *does not increase* (at least not significantly), which corresponds to a very peculiar behavior of the statistics in the nonlinear regime, as discussed in the introduction.

In figure 1, some analytical fits based on two different approaches are also shown. In each panel, the thick long dashes were calculated from

$$n_{\text{eff}}^{\text{I}}(\sigma) = n_{\text{linear}} + (n_{\text{nonlinear}} - n_{\text{linear}})x^\tau / (x^\tau + x^{-\tau}), \quad (11)$$

with

$$x = \exp \left[ \log_{10}(\sigma^2 / \sigma_0^2) \right]. \quad (12)$$

Table 1 gives the corresponding values of the parameters  $n_{\text{nonlinear}}$ ,  $\tau$  and  $\sigma_0$  as functions of  $n_{\text{linear}}$ . In equation (11), we impose that the index  $n_{\text{eff}}$  reaches a constant plateau at large  $\sigma$ ,  $n_{\text{nonlinear}}$ . The parameter  $\sigma_0$  gives the position of the transition between the linear value and the nonlinear value, and  $\tau$  defines the width of this transition.

Alternatively it is possible to allow  $n_{\text{nonlinear}}$  to have a residual  $\sigma$  dependence like the one found in CBH. The thick short dashes in Figure 1 use the following interpolation formula

$$n_{\text{eff}}^{\text{II}}(\sigma) = n_{\text{eff}}^{\text{I}}(\sigma) + [n_{\text{nonlinear}}(\sigma) - n_{\text{eff}}^{\text{I}}(\sigma)] x / (x + 1/x). \quad (13)$$

The parameter  $x$  is given by equation (12) with  $\log_{10} \sigma_0^2 = 1.8, 1.8, 2.2$  and  $3$  respectively for  $n = -2, -1, 0$  and  $+1$ , and the function  $n_{\text{nonlinear}}(\sigma)$  is

$$n_{\text{nonlinear}}(\sigma) = \frac{34}{7} - 3 - \tilde{S}_3(\sigma^2/100)^{0.045}, \quad (14)$$

where  $\tilde{S}_3$  is the value of  $S_3^{\text{meas}}$  for  $\sigma = 10$  found by CBH. (We have  $\tilde{S}_3 = 10.3, 4.8, 3$  and  $2.4$  respectively for  $n_{\text{linear}} = -2, -1, 0$  and  $+1$ ).

The two fits (11) and (13), designated hereafter respectively by I and II, are thus based on different theoretical prejudices. They both suppose that PT predictions are verified in the weakly nonlinear regime  $\sigma^2 \ll 1$ . Model I assumes moreover that the stable clustering hypothesis applies for  $\sigma^2 \gg 1$ , i.e. that the functions  $S_q$  do not depend on scale (or on  $\sigma$ ) in the highly nonlinear regime. Of course, this implies that  $n_{\text{eff}}$  becomes asymptotically constant at large  $\sigma$ , and equal to  $n_{\text{nonlinear}}$ . Model II takes into account the slight deviation from a constant found by CBH for the functions  $S_q^{\text{meas}}$  in the highly nonlinear regime, namely

$$S_q^{\text{meas}} \propto \sigma^{2 \times 0.045(q-2)}. \quad (15)$$

Note that such a power-law behavior is actually incompatible with the existence of a universal function  $n_{\text{eff}}(\sigma)$ . On the other hand, this inconsistency is very mild and produces deviations from property (9) well below the uncertainties in the

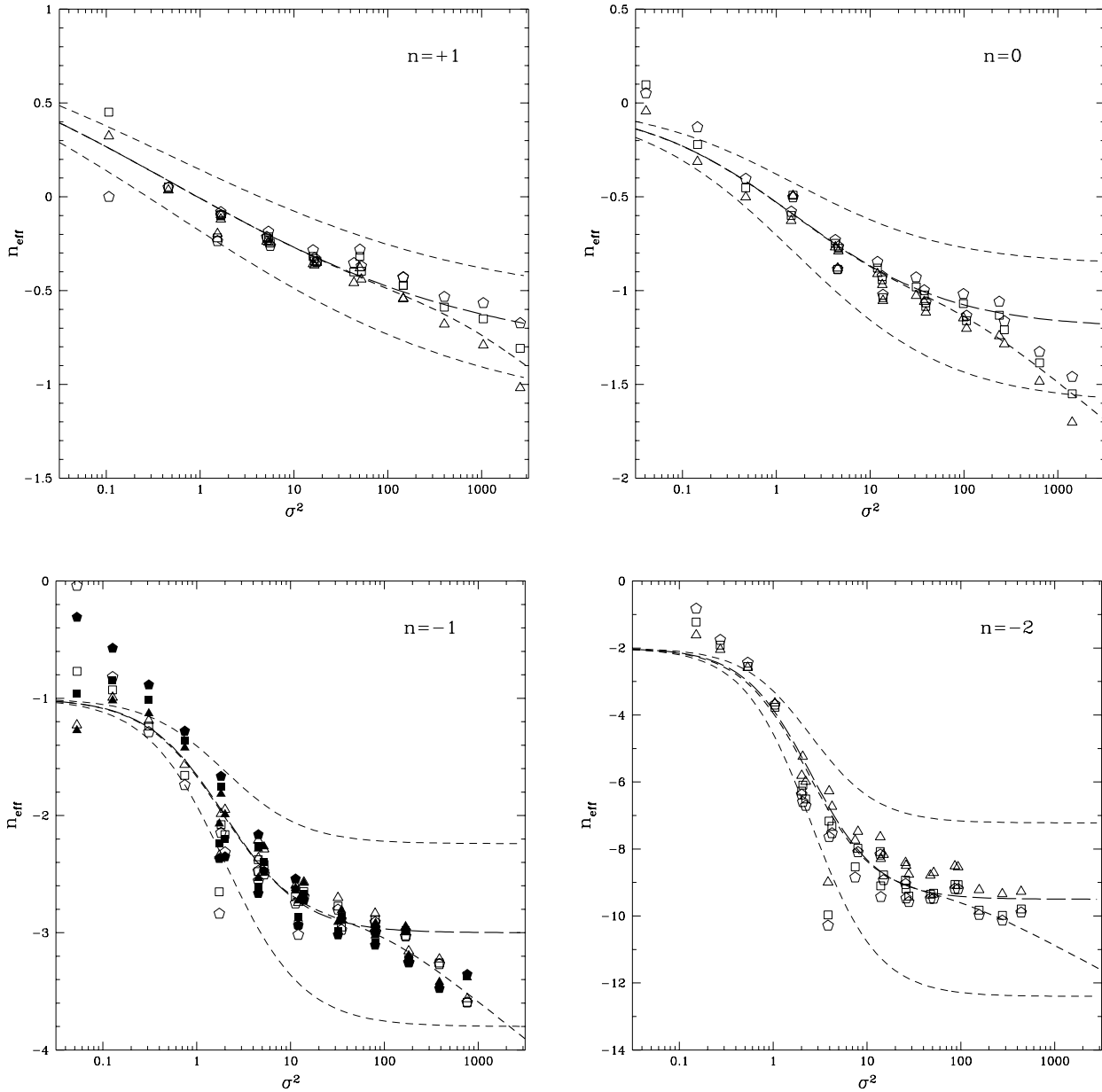


**Figure 1.** The measured spectral indices  $n_q$  obtained by inverting equations (5) (triangles), (6) (squares) and (7) (pentagons), using the values of  $S_q^{\text{meas}}$  measured by CBH. Each panel corresponds to a different value of the initial spectral index  $n_{\text{linear}}$ . In the case  $n_{\text{linear}} = -1$ , two simulations have been used (open and filled symbols). In each panel, the thick long dashed curve uses equation (11) with the parameters given in Table 1. The thin short-dashed curves bracket the range of possible fits, given the uncertainties in the measurements (see text). The thick short-dashed curves use the prejudice (14) for the large  $\sigma$  behavior of  $n_{\text{nonlinear}}$  (see text).

measurements. Such disagreement could explain, however, the slight broadening of the vertical scatter of the points at very large  $\sigma$  for  $n = 0$  and  $n = +1$ .

Figure 1 also contains two thin short-dashed curves above and below the thick long-dashed one. They use the same parameterization (11), but with different values of  $n_{\text{nonlinear}}$ , which we denote  $n_{\text{nonlinear}}^-$  and  $n_{\text{nonlinear}}^+$  for the upper and the lower curves respectively. To some extent, they bracket the domain of possible values of  $n_{\text{eff}}$ , given the uncertainties in the measurements. The numbers  $n_{\text{nonlinear}}^\pm$

come from estimates of the errors in the measurements  $S_q^{\text{meas}}$  of the parameters  $S_q$  by CBH as follows. In the nonlinear regime, such errors can be described as  $S_q^{\text{meas}}(\sigma) = S_q(\sigma) f_q^{\pm 1} \equiv S_q^\pm$ . The values of the uncertainty factors  $f_q$  are given by CBH. We take  $n_{\text{nonlinear}}^\pm \equiv \langle n_q^\pm \rangle_{q=3,4,5}$  where  $n_q^\pm$  is the function inferred from  $S_q^\pm$ , assuming that  $S_q$  is calculated from equations (5), (6) and (7) by replacing  $n_{\text{linear}}$  with the value of  $n_{\text{nonlinear}}$  given in Table 1.

The lower panels of Figure 1 contain symbols that are significantly outside the range defined by the two thin

dashed curves, at  $\sigma^2 \ll 1$  and for  $\sigma^2$  of the order of few units. In the first case, this is because our estimate of the errors tends to zero in the weakly nonlinear regime, since we assume that  $n_{\text{eff}}$  reaches  $n_{\text{linear}}$ . In the second case, the method used by CBH to correct for finite volume effects can be used only when  $\sigma^2$  is much larger than unity. As a result, it is quite difficult to apply it accurately in the regime where  $\sigma^2$  is only a few units.

## 2.2 The probability distribution function

As described in the previous section, we find that the first few moments of the PDF are well fitted by the predictions of EPT when the spectral index and the variance are allowed to be adjustable parameters. To see whether this property holds at higher order, we compare in Figure 2 the measured CPDF in our  $N$ -body sets (tiny squares) to what is predicted by EPT (solid curves), for various values of  $\sigma$  and average number of object per cell

$$\langle N \rangle \equiv \sum_{N=0}^{\infty} N P_N \quad (16)$$

(see Table 2). The details of the computations of the PDF in the EPT framework are given in detail in Appendix A. To obtain the CPDF, one convolves the final result with a Poisson distribution (see, e.g., Coles & Jones 1991). Concerning the function  $n_{\text{eff}}(\sigma)$ , we take the fit (11) with the parameters given in Table 1. The dashed curves use the functions  $n_{\text{eff}}(\sigma)$  corresponding to the thin short-dashed curves in Figure 1. To some extent, they reflect the uncertainty in the value of  $n_{\text{eff}}$ . However, there are other significant sources of error, which we list here:

- There is an uncertainty in the value of  $\sigma$  used to compute the CPDF in the EPT framework, since we use  $\sigma$  as measured in the  $N$ -body experiments. For  $n_{\text{linear}} \geq -1$ , the error in this estimate is expected to be rather small, less than or of order 30%. For  $n_{\text{linear}} = -2$ , finite volume effects strongly contaminate the measurements (CBH). In that case, we take the polynomial fit for  $\sigma^2$  (as a function of scale) in logarithmic coordinates computed by CBH, which is expected to give values of  $\sigma^2$  correct to  $\sim 30\%$ . We do not take explicitly into account the uncertainty in the measurement of  $\sigma$  in what follows, although it is by definition a requirement to know  $\sigma$  accurately for EPT to give sensible predictions. Indeed, since the variance strongly influences the shape of the PDF, particularly its width, it is obvious that two PDFs with different values of  $\sigma^2$  cannot be expected to agree with each other (unless one considers a finite range of values of  $\rho$  for the comparison).

- There is an uncertainty in the measurement of the CPDF itself. In particular, the tails of the CPDF are subject to a variety of spurious effects (discussed in detail in CBSI, CBSII and CBH): (i) some memory of the pattern used to set up the initial conditions is likely to be preserved during the simulation, particularly in under-dense regions. In our case, particles are initially perturbed from a mesh, inducing *grid effects* which are expected to alter the measured CPDF at small values of  $N$ , increasing with  $-n_{\text{linear}}$  (CBH). These effects can in principle be avoided by using

**Table 2.** Values of  $\sigma$  and  $\langle N \rangle$  used for the curves in Figure 2.

$n_{\text{linear}}$	curves	(a)	(b)	(c)	(d)	(e)
-2	$\sigma$	1.49	5.28	5.1	16.2	
	$\langle N \rangle$	1100	4.37	0.276	0.0174	
-1	$\sigma$	0.57	0.56	3.72	3.36	17.94
	$\langle N \rangle$	1100	69.3	4.37	0.276	0.0174
0	$\sigma$	0.38	3.67	3.46	22.9	
	$\langle N \rangle$	1100	4.37	0.276	0.0174	
1	$\sigma$	0.32	4.19	4.0	30.3	
	$\langle N \rangle$	1100	4.37	0.276	0.0174	

a “glass” to generate initial conditions<sup>‡</sup> (White 1994). (ii) Because of the finite size of the simulation box, the large- $N$  tail of the CPDF is dominated by a few rare clusters, inducing larger and larger (spurious) fluctuations in the CPDF as  $N$  increases, followed by a sharp cut-off.

With this in mind, we see that the agreement between EPT and the measurements is excellent, except for  $n_{\text{linear}} = -2$ , a case we discuss further below. There are some very small discrepancies at the largest value of  $\sigma$  we analyzed for  $n_{\text{linear}} = 0$  and 1 [right curves of top panels of Fig. 2, with label (d)]. Otherwise, the solid curves almost exactly superpose on the small squares.

For  $n_{\text{linear}} = -2$ , there are some significant disagreements between EPT and the measurements. While the measured high- $N$  tail of the CPDF is quite well described by EPT, there is disagreement in the second curve from the bottom [label (b)], where the shape of the CPDF predicted by EPT appears to be incorrect at small and moderate  $N$ . For the lowest curve [label (a)], the agreement between EPT and measurements is not as bad as it looks, given the uncertainties in the function  $n_{\text{eff}}$  and the large errors in the measured CPDF arising from finite volume effects. This is actually not surprising since the results are nearly in the weakly nonlinear regime where PT is expected to apply.

To summarize our  $n_{\text{linear}} = -2$  analysis, EPT does not seem to describe very well what is happening at small and moderate  $N$ , i.e. in under-dense regions, but is still quite accurate for large values of  $N$ , i.e. in over-dense regions. This result is not in contradiction with the fact that we infer a single function  $n_{\text{eff}}(\sigma)$ . Indeed, we measure it from low-order moments of the CPDF, which are dominated by the large- $N$  tail of the CPDF, increasingly so with the order  $q$ .

## 2.3 Application to non power-law spectra

The previous results apply to scale-free power spectra with particular values of  $n_{\text{linear}}$ . The first step to generalize them to arbitrary (Gaussian) initial conditions is to extrapolate them to other values of  $n_{\text{linear}}$ . Here, we propose a series of simple fits for the values of the parameters  $n_{\text{nonlinear}}$ ,  $\sigma_0$  and

<sup>‡</sup> Of course, this procedure does not correct for the discrete nature of the simulated data but keeps the white noise level of the particles as low as possible, without introducing grid effects (see, e.g., Baugh et al. 1995).

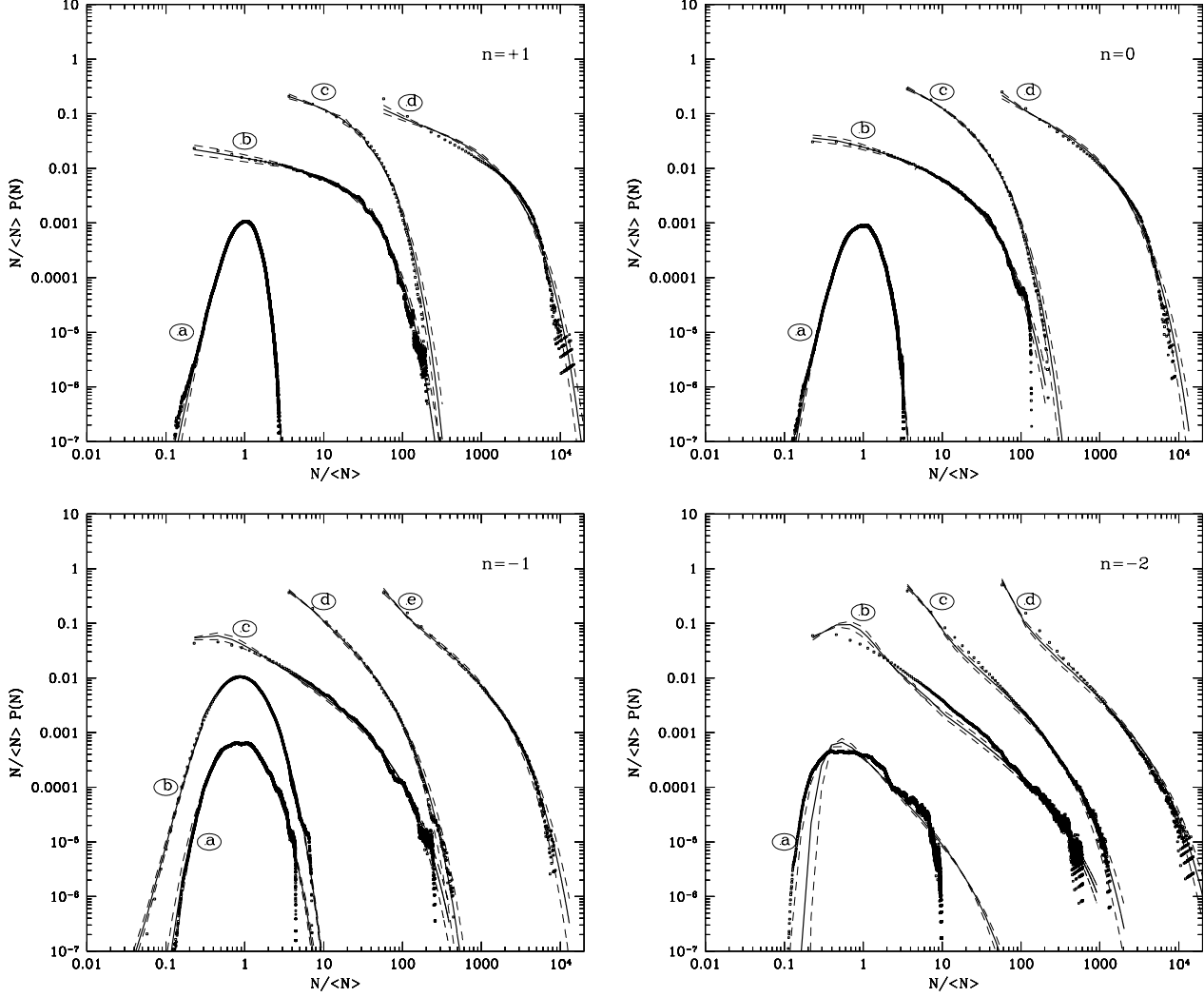


**Figure 2.** The measured CPDF as a function of  $N/\langle N \rangle$  (small squares) for various values of  $\langle N \rangle$  and  $\sigma$  (see Table 2), where  $\langle N \rangle \equiv \sum_N N P_N$  is the average number of objects per cell. Each panel corresponds to a different value of  $n_{\text{linear}}$ . The predicted CPDF from extended perturbation theory (eq. [10]) (solid curve), is calculated assuming that the function  $n_{\text{eff}}(\sigma)$  is given by equation (11) with the parameters displayed in Table 1. The two dashed curves bracketing the solid one correspond to the upper and the lower thin dashed curves in Figure 1.

$\tau$ , of fit I as functions of  $n_{\text{linear}}$ :

$$n_{\text{nonlinear}}(n_{\text{linear}}) = \frac{3(n_{\text{linear}} - 1)}{3 + n_{\text{linear}}} \quad (17)$$

$$\tau(n_{\text{linear}}) = 0.8 - 0.3 n_{\text{linear}} \quad (18)$$

$$\log_{10} \sigma_0^2(n_{\text{linear}}) = 0.2 - 0.1 n_{\text{linear}} \quad (19)$$

As can be seen from Figure 3, these fits reproduce well the values found for  $n_{\text{linear}} = -2, -1$  and  $0$ , but are less accurate for  $n_{\text{linear}} = +1$ . In any event, the values of cosmological interest are within the range  $n_{\text{linear}} \leq 0$ . Figure 4 shows the quantities  $n_{\text{eff}}$  obtained for different values of the index  $n_{\text{linear}}$  as functions of the variance (solid lines). [The interrelations (17), (18) and (19) are used only for  $n_{\text{linear}} = -0.5$  and  $n_{\text{linear}} = -1.5$ .]

Note that Fry, Mellot & Shandarin (1993) measured  $S_3 \simeq 9/(3 + n_{\text{linear}})$  in the highly nonlinear regime, which implies  $n_{\text{nonlinear}} \simeq (1.9n_{\text{linear}} - 2.5)/(3 + n_{\text{linear}})$ , a formula very similar to equation (17). This equation diverges for

$n_{\text{linear}} = -3$ , implying that equation (17) is probably valid only for  $-3 < n_{\text{linear}} \lesssim 0$ .

Now, we can generalize the above results to scale dependent power-spectra. This is actually not completely straightforward. For scale-free initial conditions, a single parameter  $n_{\text{linear}}$  can be used to entirely describe the shape of the initial power-spectrum. For more complex initial conditions, such as CDM, PT predictions require not only a knowledge of  $-(n_{\text{linear}} + 3) = d \log \sigma_{\text{linear}}^2 / d \log \ell$ , but also of higher logarithmic derivatives of the linear variance with respect to the filtering scale

$$\gamma_p \equiv \frac{d \log^p \sigma_{\text{linear}}^2}{d \log^p \ell}, \quad p \geq 2. \quad (20)$$

For example, equation (6) must now include a term depending on  $\gamma_2$  and more generally, the ratio  $S_q$  involves  $\gamma_p$  terms for  $p \leq q-2$ . It was, however, noticed by Bernardeau (1994b) that for CDM like power spectra, such corrections can be ne-

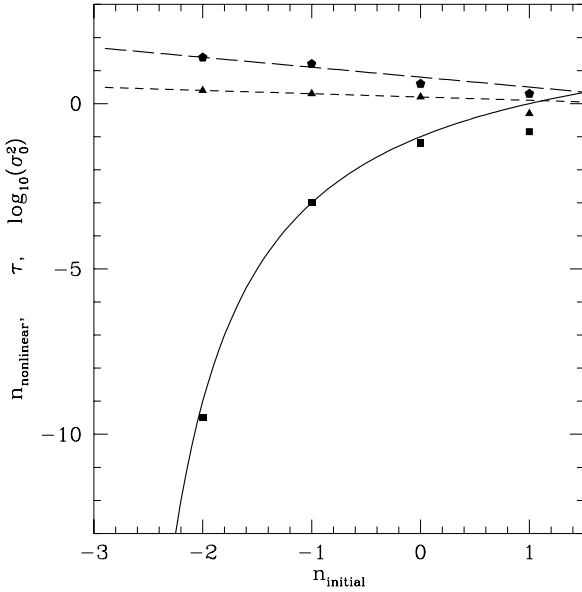


**Figure 3.** The  $n_{\text{linear}}$  dependence of the parameters  $n_{\text{nonlinear}}$  (squares),  $\tau$  (pentagons) and  $\log_{10} \sigma_0^2$  (triangles) used in the fit I [eq. (11)]. The symbols correspond to the values given in Table 2. The solid curve, long dashes and short dashes correspond to the simple analytical forms (17), (18) and (19) respectively.

glected for  $S_q$ ,  $q \leq 4$ , i.e., one can take  $\gamma_p = 0$  for  $p \geq 2$ , while still preserving reasonable accuracy. This may not be true when higher order moments must be predicted accurately. Baugh et al. (1995) took into account  $\gamma_p$  for  $p \leq 3$  to predict  $S_q$  up to  $q = 10$ . But these are tiny refinements and it has been shown that, in the weakly nonlinear regime, the shape of the PDF is quite well reproduced when only the local index  $n_{\text{linear}}$  is used (B94). There is no reason why this should also be the case in the EPT framework, but we can assume that it is so and check this hypothesis directly by measuring the functions  $n_q$  in simulations with scale-dependent initial conditions.

Figure 4 displays the functions  $n_q(\sigma)$  obtained from two CDM simulations with different box sizes (by Davis & Efstathiou 1988 and Frenk et al. 1990), using measurements of the ratios  $S_3$  (triangles),  $S_4$  (squares) and  $S_5$  (pentagons) by CBSI. Again, as in Figure 1, the quantities  $n_q$  superpose to define a unique function  $n_{\text{eff}}(\sigma)$ , in agreement with EPT.

Now it remains to be seen whether one can infer the function  $n_{\text{eff}}(\sigma)$  from our results for scale-free power-spectra [using eqs. (17), (18) and (19)]. The problem is that the quantity  $n_{\text{linear}}$  now depends on scale. In the weakly nonlinear regime, we have of course

$$n_{\text{linear}}(\ell) = -\gamma_1(\ell) - 3, \quad \sigma^2 \ll 1. \quad (21)$$

But in the nonlinear regime there is an ambiguity concerning the scale at which the initial index should be chosen. We consider two simple options:

- (A) With an Eulerian approach, one would generalize formula (21) to any value of  $\sigma$ .
- (B) Within a Lagrangian framework, one would rather choose  $n_{\text{linear}}$  according to

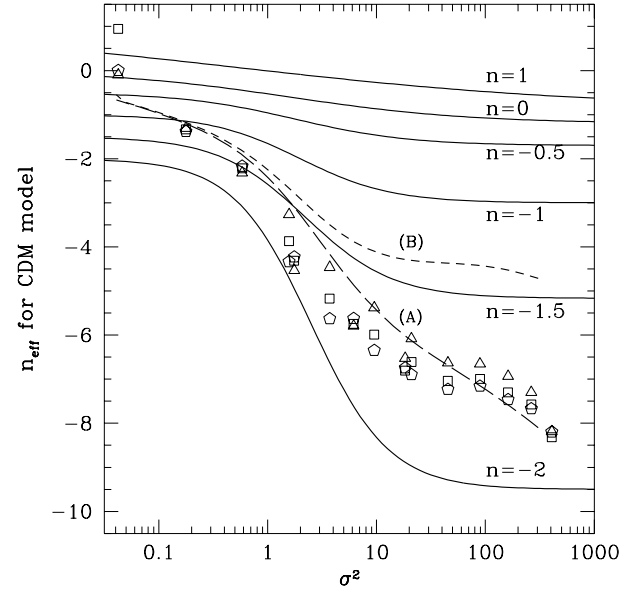


**Figure 4.** The effective index for the CDM model. The triangles, squares and pentagons correspond to the measured functions  $n_q(\sigma)$  for  $q = 3, 4$  and  $5$  respectively. The solid lines correspond to our phenomenological fit  $n_{\text{eff}}^I$  for scale-free initial conditions [eq. (11)] with parameters given by Table 1, and by eqs. (17), (18) and (19) for  $n_{\text{linear}} = -0.5$  and  $n_{\text{linear}} = -1.5$ . The numbers  $n$  on the figure stand for  $n_{\text{linear}}$ . The long dashes correspond to the prediction for CDM using the prescription (A) and the short dashes use the prescription (B) (see text).

$$n_{\text{linear}}(\ell) \equiv -\gamma_1(\ell_s) - 3, \quad (22)$$

where the scale  $\ell_s$  is related to  $\ell$  in the same way as in the Hamilton et al. (1991) prescription for the transform function of the variance, i.e.

$$\ell_s^3 \approx \ell^3 (1 + \sigma^2). \quad (23)$$

Of course, we have  $\ell_s \simeq \ell$  when  $\sigma^2 \ll 1$ , in agreement with equation (21).

In Figure 4, we compare the prescriptions (A) (long dashes) and (B) (short dashes) to our measurement of function  $n_{\text{eff}}(\sigma)$ . The first prescription appears to be clearly better than the second. This is somewhat surprising since prescription (B) is expected to be more “physical” than (A). Further investigations are required to understand the implications of this result.

### 3 THE DENSITY PDF IN THE HIGHLY NONLINEAR REGIME

In the continuous limit, and in the highly nonlinear regime, one can use PT results to compute some simple analytical properties of the PDF in the EPT framework. Indeed, as we are going to see in § 3.1, the full shape and properties of the PDF in this regime can be simply described by a few parameters, which are of course all fixed by the value of  $n_{\text{eff}}$ . One can thus check EPT predictions by measuring, if possible, these parameters directly from the shape of the

PDF, and by comparing the results with what would be obtained with the values of  $n_{\text{eff}}$  we measured in § 2.1. This analysis, which is the subject of § 3.2, should confirm the results of § 2.2.

### 3.1 EPT results

Here, extrapolating the PT calculations of B94 to the highly nonlinear regime (i.e. assuming  $S_q \equiv S_q^{\text{PT}}$ ), we sketch simple analytical properties of the density PDF in the EPT framework, when the variance is large. Details are given in Appendix A. Let us just recall that in the continuous limit, the shape of the density PDF is related to two functions  $g(z)$  and  $h(x)$ , which are both entirely determined from the expression of the generating function of the  $S_q$  parameters (BS). Their respective domains of validity are bounded by

$$\rho_o = \sigma^2 \quad (24)$$

and

$$\rho_u = a^{1/(1-\omega)} \sigma^{2\omega/(\omega-1)}, \quad (25)$$

where the parameters  $a$  and  $\omega$  are set by the value of  $n_{\text{eff}}$  (see Table 3 for numerical values and Appendix A.1 for analytical expressions of  $a$  and  $\omega$ ). There are two regimes:

$$P_{\text{PT}}(\rho, \sigma, n_{\text{eff}}) \simeq \frac{1}{\rho_u} g\left(\frac{\rho}{\rho_u}\right), \quad \text{when } \rho \ll \rho_o, \quad (26)$$

and

$$P_{\text{PT}}(\rho, \sigma, n_{\text{eff}}) \simeq \frac{1}{\rho_o^2} h\left(\frac{\rho}{\rho_o}\right), \quad \text{when } \rho \gg \rho_u. \quad (27)$$

These regimes actually overlap in the region  $\rho_u \ll \rho \ll \rho_o$  when the variance is large. In this interval, functions  $g$  and  $h$  exhibit the same power law behavior. Note that the global shape of  $g(z)$  depends only on the value of  $\omega$  (see BS, B94 and Appendix A). It exhibits an exponential cut-off at small  $z$ . The function  $h(x)$  is more complex and depends on the whole shape of the generating function of  $S_q$ . It is expected to exhibit the following power-law behavior at small  $x$

$$h(x) \simeq a \frac{(1-\omega)}{\Gamma(\omega)} x^{\omega-2}, \quad x \ll 1, \quad (28)$$

and an exponential tail at large  $x$

$$h(x) \simeq \frac{3a_s}{4\sqrt{\pi}} x^{-5/2} \exp(-|y_s|x), \quad x \gg 1. \quad (29)$$

Again, the parameters  $y_s$  and  $a_s$  are entirely fixed by the value of  $n_{\text{eff}}$  (see Table 3 and Appendix A.1 for the analytical expression of  $y_s$ ).

Figure 5 shows the functions  $z^2 g(z)$  and  $x^2 h(x)$  [numerically obtained from equations (47) and (49) in Appendix A.1] in logarithmic coordinates for various values of  $n_{\text{eff}} = -9, -3, -1$  and  $-0.5$ . These are approximately the values of  $n_{\text{eff}}(\sigma)$  we measured in our scale-free simulations at  $\sigma = 10$  for  $n_{\text{linear}} = -2, -1, 0$  and  $+1$  respectively.

### 3.2 Comparisons with $N$ -body Results

As for the CPDF in § 2.2, we can check the validity of EPT by testing directly the analytical forms of § 3.1 in our  $N$ -body simulations. In particular, we can try to measure the

**Table 3.** Parameters  $\omega$ ,  $a$ ,  $a_s$  and  $|y_s|$  for various values of the spectral index  $n_{\text{eff}}$ .

$n_{\text{eff}}$	$\omega$	$a$	$a_s$	$1/ y_s $
-0.5	0.6667	2.044	18.94	1.7436
-1	0.6000	2.104	6.677	2.4923
-2	0.5000	2.121	2.809	3.9574
-3	0.4286	2.082	1.842	5.4112
-4	0.3750	2.025	1.413	6.8614
-5	0.3333	1.966	1.169	8.3100
-6	0.3000	1.908	1.012	9.7576
-7	0.2727	1.855	0.900	11.205
-9	0.2308	1.763	0.752	14.098
-11	0.2000	1.689	0.657	16.991

parameters fixing the shape of the functions  $g$  and  $h$  (if they exist, of course), and compare the results with what would be obtained from the values of  $n_{\text{eff}}$  we measured in § 2.1. This analysis should confirm the results of § 2.2. However, it is not easy to carry this out, for several reasons:

- The effective power index  $n_{\text{eff}}$  can vary with  $\sigma$  even in the highly nonlinear regime, which would render the comparisons with EPT quite difficult, since each value of the variance should be considered independently. However this variation is, as discussed in CBH and in § 2.1, quite weak, and  $n_{\text{eff}}$  can be taken to be constant to a first order of approximation.

- Strictly speaking, the continuous limit is not reached in our  $N$ -body simulations. Discreteness effects can significantly contaminate the measurements, even in samples with  $\sim 3 \times 10^5$  objects like our  $N$ -body sets. Fortunately one can correct for them (at least partially), as proposed by Bouchet, Schaeffer & Davis (1991, hereafter BSD).

- As discussed in § 2.2, other spurious effects, such as grid effects at small  $N$  and more importantly finite volume effects at large  $N$  can significantly affect the measurements.

Except for the first point above, these problems have been extensively discussed in BSD, Bouchet & Hernquist (1992, hereafter BH) and particularly in CBSII. We refer the reader to these papers for details concerning the practical measurement of the functions  $g$  and  $h$ .

Although we do not find it necessary to present the results here, we find a remarkable qualitative agreement between the measurements and the predictions (26) and (27) in the regime  $\sigma^2 \gg 1$ , after the appropriate corrections. Aside from the case  $n_{\text{linear}} = +1$ , and to a lesser extent  $n_{\text{linear}} = 0$ , the scale dependence of  $n_{\text{eff}}$  cannot really be neglected (see Fig. 1).

We also tried to estimate by direct measurements (see, e.g., BSD, BH, CBSII) the most important parameters of the functions  $g$  and  $h$ , i.e.  $\omega$  and  $|y_s|$ . The first one,  $\omega$ , indeed completely determines the behavior of the PDF around its maximum and in under-dense regions, and the second one,  $|y_s|$ , determines the high-density tail of the PDF, therefore influencing enormously the values of the moments of the PDF. The parameter  $\omega$  is thus estimated by studying the small- $N$  behavior of the CPDF (through an estimator of the function  $g$ , using the corrections for discreteness proposed by BSD), whereas  $|y_s|$  is estimated by analyzing the large- $N$  behavior of the CPDF (through an estimator of



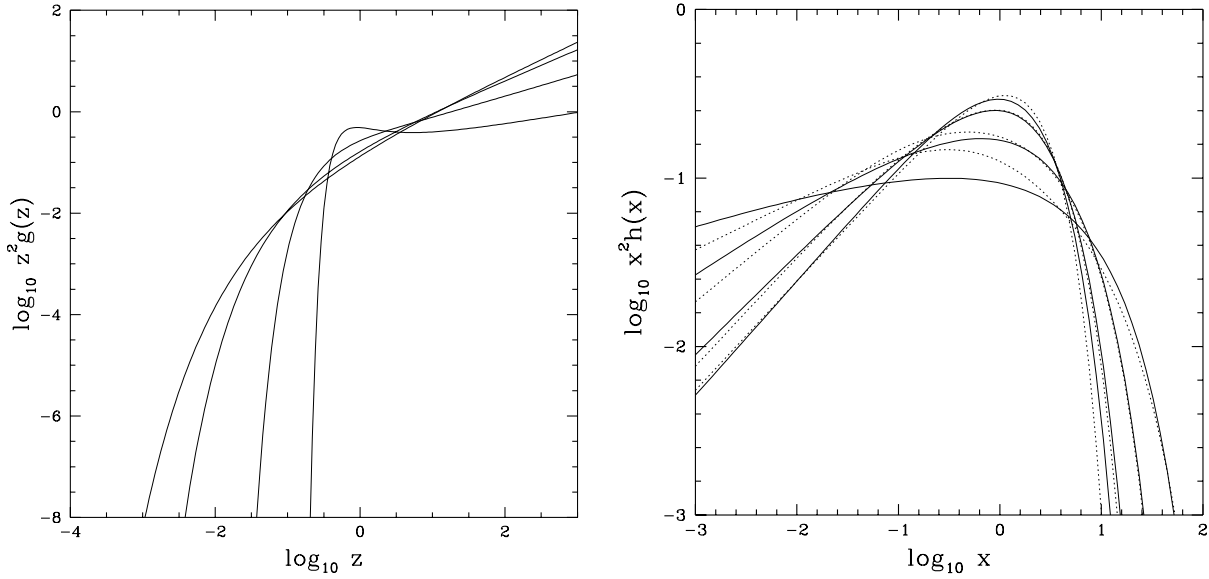


**Figure 5.** The functions  $z^2g(z)$  (left panel) and  $x^2h(x)$  (right panel), in logarithmic coordinates, for various values of  $n_{\text{eff}} = -0.5, -1, -3$  and  $-9$  (solid curves). When  $n_{\text{eff}}$  decreases, the exponential tail of the function  $z^2g(z)$  at small  $z$  becomes sharper and the power-law at large  $z$  less steep. The maximum of  $x^2h(x)$  increases with  $n_{\text{eff}}$ . The dashed curves are the “preferred” fits of the function  $h$  measured in our  $N$ -body simulations, using equation (30) with  $a, b, c, \omega$  and  $|y_s|$  as adjustable parameters. If EPT applies, each dashed curve should, within measurement errors, superpose to the globally closest solid curve.

**Table 4.** Comparison between EPT and measurements in our  $N$ -body simulations for  $\omega$  and  $|y_s|$ .

$n_{\text{linear}}$	$n_{\text{eff}}$	$\omega(g)$	$\omega(n_{\text{eff}})$	$1/ y_s(h) $	$1/ y_s(n_{\text{eff}}) $
-2	$-9 \pm_{0.75}^{2.18}$	$0.3 \pm_{0.03}^{0.05}$	$0.23 \pm_{0.04}^{0.05}$	$18 \pm_6^2$	$14 \pm_3^4$
-1	$-3 \pm_{0.79}^{0.67}$	$0.5 \pm 0.05$	$0.43 \pm 0.04$	$5 \pm_{0.5}^1$	$5.4 \pm_{1.2}^1$
0	$-1 \pm_{0.36}^{0.32}$	$0.65 \pm_{0.1}^{0.15}$	$0.6 \pm 0.04$	$2 \pm_{0.2}^{0.5}$	$2.5 \pm 0.5$
+1	$-0.5 \pm_{0.28}^{0.24}$	$0.65 \pm_{0.05}^{0.35}$	$0.67 \pm_{0.04}^{0.03}$	$1 \pm_0^{0.5}$	$1.74 \pm 0.4$

the function  $h$ , using the corresponding BSD corrections for discreteness). Table 4 summarizes the results of our measurements ( $\omega(g), 1/|y_s(h)|$ ), compared with what is obtained from equations (40) and (42) in Appendix A.1 taking for  $n$  the value of  $n_{\text{eff}}$  we measure from quantities  $S_Q$  at  $\sigma^2 \sim 100$  ( $\omega(n_{\text{eff}}), 1/|y_s(n_{\text{eff}})|$ ).

The agreement between both estimates of  $\omega$  and  $|y_s|$  is quite good, as expected if EPT applies. There is a small problem in the case  $n_{\text{linear}} = -2$ , where the measured  $\omega$  seems larger than the one given by EPT (but the error bars on each estimate overlap). The same effect exists for  $n_{\text{linear}} = -1$ , but it is less significant.

We also tried to find a best fit for the function  $h$ , using the parameterization proposed by BSD, i.e.

$$h_{\text{fit}}(x) = a \frac{(1-\omega)}{\Gamma(\omega)} x^{\omega-2} (1+bx)^{-c} \exp(-|y_s|x), \quad (30)$$

with  $a, b$  and  $c$  being *adjustable* parameters<sup>§</sup>, and with our “preferred” values of  $\omega$  and  $|y_s|$  obtained from the direct measurement of the functions  $g$  and  $h$ . The resulting parameters are listed in Table 5. We obtained the dotted curves in the right panel of Figure 5, which compare well with the predictions from EPT, with our “preferred” measured value of  $n_{\text{eff}}$  at  $\sigma^2 \sim 100$ , particularly for the large- $x$  exponential tail. The agreement with EPT is not that good at small  $x$  for  $n_{\text{eff}} = -9$  ( $n_{\text{linear}} = -2$ ) and is marginal for  $n_{\text{eff}} = -3$

<sup>§</sup> Note that, in principle, in equation (30), the parameters  $a, b$  and  $c$  are entirely determined in the EPT framework. The number  $a$  is indeed given by equation (39) in Appendix A.1 and from equation (29), we get

$$c = \omega + 1/2, \quad (31)$$

$$b = \left[ \frac{4\sqrt{\pi}a(1-\omega)}{3a_s\Gamma(\omega)} \right]^{1/(\omega+1/2)}. \quad (32)$$

However, with such values of  $a, b$  and  $c$ , the simple analytical form (30) approximates the exact EPT result satisfactorily only for  $n_{\text{eff}} > -2$ . At the degree of approximation we consider here, it is thus better to keep  $a, b$  and  $c$  as free parameters.

**Table 5.** Our preferred values of  $a$ ,  $b$ ,  $c$ ,  $\omega$  and  $|y_s|$  in equation (30) as we measure functions  $g$  and  $h$ .

$n_{\text{linear}}$	$a$	$b$	$c$	$\omega$	$1/ y_s $
-2	1.273	1.455	0.9	0.3	18
-1	2.068	4.3	0.6	0.5	5
0	2.7	8	0.225	0.65	2
+1	1.937	0.486	-1.35	0.65	1

( $n_{\text{linear}} = -1$ ). Of course, all these measurements are quite delicate and the uncertainties are large. However, the disagreement for  $n_{\text{eff}} = -9$  is quite consistent with the conclusions of § 2.2.

Thus, the results of this section corroborate those of § 2.2, as expected.

#### 4 DISCUSSION

In this paper, we have studied the probability distribution function (PDF) of the density field smoothed with top hat windows in  $N$ -body simulations with scale-free initial conditions and linear spectral indices  $n_{\text{linear}} = -2, -1, 0$  and  $+1$ . We attempted to determine if the following *Extended Perturbation Theory* (EPT) applies. Such an ansatz consists of assuming that the PDF is given by  $P(\rho) = P_{\text{PT}}(\rho, \sigma, n_{\text{eff}})$ , where the function  $P_{\text{PT}}(\rho, \sigma, n_{\text{linear}})$  is the prediction of *Perturbation Theory* (PT, e.g., B94), which is valid in the weakly nonlinear regime  $\sigma \simeq \sigma_{\text{linear}} \ll 1$ . The difference with PT is that the *effective* spectral index  $n_{\text{eff}}$  is assumed to be an adjustable parameter of the model and  $\sigma^2$  is the *nonlinear* variance<sup>¶</sup>. The measurement of low-order moments of the PDF and of the PDF itself in our  $N$ -body experiments shows a remarkable agreement with EPT, except for  $n_{\text{linear}} = -2$  in some regimes. (This is however a limiting case, subject to many numerical uncertainties, particularly finite volume effects, see e.g. CBH).

As can be seen from Figure 1, the effective spectral index, equal of course to  $n_{\text{linear}}$  in the weakly nonlinear regime, decreases with  $\sigma$  to approximately reach another plateau at large  $\sigma$ . If this second plateau were completely flat, our measurements would agree with the predictions of stable clustering. This does not appear to be exactly the case, except perhaps for  $n_{\text{linear}} = -2$ , although the deviation from stable clustering is quite weak. We do not discuss this problem further here, since it was analyzed extensively in CBH. The difference between the second and the first plateau increases with  $-n_{\text{linear}}$ . For  $\sigma^2 \sim 100$ , we have for example  $n_{\text{eff}} \simeq -9, -3, -1$  and  $-0.5$  respectively for  $n_{\text{linear}} = -2, -1, 0$  and  $+1$ .

It is important to notice that the quantity  $-(3+n_{\text{eff}})$  is *different* from the logarithmic derivative of  $\sigma^2$  with respect

<sup>¶</sup> Thus, the PDF obtained from EPT has exactly the same variance as the data, by definition. This is obviously a necessary condition for agreement between theory and measurements (but not a sufficient one, in general, except of course in the Gaussian limit). This is why we think it does not make much sense to try extending PT results to the nonlinear regime by identifying the variance of the theoretical PDF with the value given by linear theory.

to scale, except of course in the weakly nonlinear regime. Indeed, as measured in  $N$ -body simulations by Efstathiou et al. (1988), CBH, and Jain (1996), the variance follows quite well the stable clustering predictions in the framework of the self-similar solution (see, e.g., Davis & Peebles 1977; Peebles 1980), in the regime  $\sigma^2 \gtrsim 100$ . In particular, we get

$$-(3+n_{\sigma}) \equiv \frac{d \log \sigma^2}{d \log \ell} \simeq -\frac{3(3+n_{\text{linear}})}{5+n_{\text{linear}}}, \quad \sigma^2 \gtrsim 100, \quad (33)$$

i.e.,  $n_{\sigma} = -2, -1.5, -1.2, -1$  respectively for  $n_{\text{linear}} = -2, -1, 0$  and  $+1$ . These values are quite different from the  $n_{\text{eff}}$  we measure.

We have tried to apply EPT to a scale dependent power-spectrum, such as CDM. The results given in Figure 4 are encouraging. However, further investigations are needed to address the case of non power-law spectra in greater detail.

Szapudi, Meiksin & Nichol (1996) have recently measured the functions  $n_q$  in the Edinburgh/Durham Southern Galaxy catalogue (EDSGC). In this angular survey, the functions  $n_q$  superpose well, given the uncertainties in the measurements, although there is a systematic increase in the scatter of values of  $n_q$  on small scales. Szapudi et al. find, as we do, that the function  $n_{\text{eff}}$  exhibits two plateaus, one on small scales where  $-7 \lesssim n_{\text{eff}} \lesssim -4$  and another on large scales where  $-2.5 \lesssim n_{\text{eff}} \lesssim -1$ , in good qualitative agreement with the results of our analysis and with what would be expected in a CDM-like universe. Of course, such a comparison is limited by the fact that there are non trivial projection effects of the galaxy distribution along the line of sight in angular surveys. Moreover, one has to keep in mind that light does not necessarily trace mass.

If EPT is indeed valid, a knowledge of the variance  $\sigma$  and of the spectral index  $n_{\text{eff}}$  is sufficient to compute the PDF. We have provided analytical fits to the function  $n_{\text{eff}}(\sigma)$ . The nonlinear variance  $\sigma^2$  can itself be calculated with other nonlinear ansatz, such as the fitting formula found by Hamilton et al. (1991) (improved later by Peacock & Dodds 1994; Jain, Mo & White 1995; Baugh & Gaztañaga 1996), provided one generalizes it to the smoothed density field.

Our analysis has been done for flat universes with density parameter  $\Omega = 1$ . PT predictions for the ratios  $S_q$  are expected to be only weakly dependent on the value of  $\Omega$  or on the cosmological constant  $\Lambda$  (e.g., Martel & Freudling 1991, Bouchet et al. 1992, 1995, Bernardeau 1992, 1994b, Hivon et al. 1995). But this does not really guaranty the existence of a universal function  $n_{\text{eff}}(\sigma)$  in the case  $\Omega \neq 1$  and/or  $\Lambda \neq 0$ . More investigations have to be undertaken in this regime.

Of course, it also remains to explain why the hierarchy of cumulants of the PDF looks similar in the weakly nonlinear and the highly nonlinear regimes. One way to address this question would be to study the transition between the two regimes, by computing higher order corrections in equation (3) (e.g., Scoccimarro & Frieman 1996; Scoccimarro 1996). Alternatively, as in the early attempts of Fry (1984) and Hamilton (1988), one could study the BBGKY equations (see, e.g., Peebles 1980) to try to find clues for the determination of the  $S_q$  parameters in the highly nonlinear regime.

## 5 ACKNOWLEDGMENTS

We thank E. Gaztañaga for useful comments. F. Bernardeau would like to thank IAP, where a large part of the work has been completed, for its warm hospitality. This work was supported in part by the Pittsburgh Supercomputing Center, the National Center for Supercomputing Applications (Illinois), the San Diego Supercomputing Center and by an allocation from the scientific counsel of IDRIS, Palaiseau. L. Hernquist acknowledges support from NASA Theory Grant NAGW-2422, and the NSF under Grant ASC 93-18185 and the Presidential Faculty Fellows Program.

## APPENDIX

### PRACTICAL CALCULATION OF THE PDF IN THE FRAMEWORK OF EXTENDED PERTURBATION THEORY

In this appendix, we first study, in the framework of EPT, the derivation of the cosmic density PDF, and its properties when the variance is large. All the results are discussed in term of the index  $n$ . For PT,  $n$  is simply the initial spectral index,  $n \equiv n_{\text{linear}}$ , and, more generally, in EPT, we have  $n \equiv n_{\text{eff}}$ . In the following we will suppose that  $n < 0$ .

#### A.1 Analytic predictions

In general the density PDF is given by an inverse Laplace transform,

$$P(\rho) \, d\rho = d\rho \int_{-\infty}^{+\infty} \frac{dy}{2\pi i \sigma^2} \exp \left[ -\frac{\phi(y)}{\sigma^2} + \frac{\rho y}{\sigma^2} \right], \quad (34)$$

where  $\phi(y)$  is the generating function of the  $S_q$  parameters [eq. (2)]:

$$\phi(y) \equiv \sum_{q=1}^{\infty} (-1)^{q-1} \frac{S_q}{q!} y^q \quad (35)$$

( $S_1 \equiv S_2 \equiv 1$ ).

In the PT framework and for scale-free initial conditions, the function  $\phi$  is determined by the following set of implicit equations<sup>||</sup> (see B94):

$$y = -\frac{3}{8}(1+\mathcal{G})^{(n-4)/3} \left[ (1+\mathcal{G})^{2/3} - 1 \right] \times \left[ (n+3)(1+\mathcal{G})^{2/3} + 1 - n \right], \quad (36)$$

$$\phi = \frac{3}{8}(1+\mathcal{G})^{(n-4)/3} \left[ (1+\mathcal{G})^{2/3} - 1 \right] \times (1+\mathcal{G}) \left[ -n(1+\mathcal{G})^{2/3} + (n-4) \right]. \quad (37)$$

The integral (34) is not easy to estimate analytically. In general, one must calculate it numerically (see section A.2). The important properties of the PDF, however, depend only on the behavior of  $\phi(y)$  at large  $y$  and near its critical point  $y_s$  (BS). The absolute value of  $y_s$  is the radius of absolute

<sup>||</sup> These equations have been obtained assuming that the spherical collapse solution is well approximated by  $\mathcal{G} = (1 - 3\delta_i/2)^{-3/2}$ , where  $\delta_i$  is the linear density contrast and  $\mathcal{G} - 1$  is the present density contrast.

convergence of the series (35). From equations (36) and (37), one can deduce that when  $y \gg 1$

$$\phi(y) \simeq ay^{1-\omega}, \quad (38)$$

with

$$a = \frac{4-n}{1-n} \left[ \frac{8}{3(1-n)} \right]^{3/(n-4)}, \quad (39)$$

and

$$\omega = \frac{3}{4-n}. \quad (40)$$

On the other hand, the behavior of  $\phi$  around  $y_s$  can be written

$$\phi(y) - \phi_s \simeq r_s(y - y_s) + a_s(y - y_s)^{3/2}. \quad (41)$$

The calculation of  $y_s$  yields

$$y_s = -\frac{3}{8}A^{-n/2}(A-1)[(n-1)A - (n+3)], \quad (42)$$

where

$$A = \frac{[(n^2 - n - 2)^2 - (n-1)(n-4)n(n+3)]^{1/2}}{(n-1)(n-4)} + \frac{n^2 - n - 2}{(n-1)(n-4)}. \quad (43)$$

The value of  $a_s$  is hard to obtain analytically and we compute it numerically for various values of  $n$  (see Table 3). A knowledge of  $\phi_s$  and  $r_s$  is not relevant here.

We can now define, following the formalism of BS, the typical density of an under-dense region as

$$\rho_u = a^{1/(1-\omega)} \sigma^{2\omega/(\omega-1)}, \quad (44)$$

and the typical density of an over-dense region as

$$\rho_o = \sigma^2. \quad (45)$$

For regions with small enough density, the PDF can be written as

$$P_{\text{PT}}(\rho, \sigma, n) \simeq \frac{1}{\rho_u} g \left( \frac{\rho}{\rho_u} \right), \quad \rho \ll \rho_o. \quad (46)$$

The shape of the function  $g(z)$  depends only on the value of the parameter  $\omega$  (BS) through the following integral

$$g(z) = \frac{1}{\pi} \int_0^{\infty} du \exp[-zu + u^{1-\omega} \cos \pi\omega] \times \sin[u^{1-\omega} \sin \pi\omega]. \quad (47)$$

It has a exponential tail at small  $z$  and a power-law behavior in  $z^{\omega-2}$  at large  $z$  (see B94 or BS for details).

For regions with large enough density, we have

$$P_{\text{PT}}(\rho, \sigma, n) \simeq \frac{1}{\rho_o^2} h \left( \frac{\rho}{\rho_o} \right), \quad \rho \gg \rho_u, \quad (48)$$

where the function  $h(x)$  is related to function  $\phi(y)$  through the following transform (BS)

$$h(x) = -\frac{1}{2\pi} \int_{-\infty}^{+\infty} du \phi(iu) e^{iux}. \quad (49)$$

It exhibits a power-law behavior (28) at small  $x$  (this regimes overlaps the large  $z$  regime of function  $g$ ) and an exponential tail at large  $x$  given by equation (29). Note that the parameters  $S_q$  are simply the moments of the function  $h$ ,

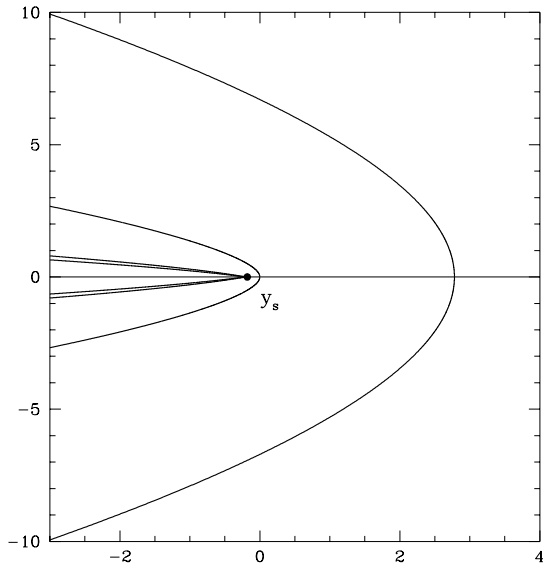


**Figure 6.** Example of paths in the complex plane for  $y$ . The parameters correspond to  $n = -3$  and  $\sigma = 1$ . The paths cannot cross the real axis for  $y < y_s$ . When the density is small, the paths are on the right side. When the density is large, they are on the left side and cross the real axis at  $y = y_s$ .

$$S_q = \int_0^{\infty} x^q h(x) dx, \quad (50)$$

and we have the following normalizations

$$\int_0^{\infty} x h(x) dx = \int_0^{\infty} x^2 h(x) dx = 1. \quad (51)$$

## A.2 Numerical Integration

The starting point of the numerical calculation of the density PDF is equation (34). Since the intervening quantities are all known as functions of  $\mathcal{G}$ , this latter is our natural variable of integration. The expression for the density PDF thus reads,

$$P(\rho) d\rho = d\rho \int_{-i\infty}^{+i\infty} \frac{d\mathcal{G}}{2\pi i \sigma^2} \frac{dy(\mathcal{G})}{d\mathcal{G}} \times \exp \left[ -\frac{\phi(y)}{\sigma^2} + \frac{\rho y}{\sigma^2} \right]. \quad (52)$$

The difficult part of the integration is to choose the proper path in the complex plane. The original path for  $y$  runs from  $-i\infty$  to  $+i\infty$  along the imaginary axis. But as the functions  $\tau(y)$  or  $\phi(y)$  are not analytic in  $y$ , there is at least one singularity on the real axis for  $y = y_s$  ( $< 0$ ), and it is impossible to move the path to the left of this singularity.

Actually, the starting point of the path for the numerical integration is the position of the saddle point,  $y_{\text{saddle}}$  defined by

$$0 \equiv \rho - \left. \frac{d\phi(y)}{dy} \right|_{y=y_{\text{saddle}}}. \quad (53)$$

If there is no solution, that is when  $\rho > 1 + \mathcal{G}_s$  for  $y(\mathcal{G}_s) = y_s$ , the starting point is the singular point  $y_s$ . Then, the

path is chosen in such a way that  $\phi(y) + \rho y$  is kept real to avoid unnecessary oscillation of the integrand. Using this prescription, followed with an adaptive step, the paths that are found are similar to the ones shown in Figure 6.

## REFERENCES

- Alimi J.-M., Blanchard A., Schaeffer R., 1990, *ApJ*, 349, L5  
 Balian R., Schaeffer R., 1989, *A&A*, 220, 1 (BS)  
 Baugh C.M., Gaztañaga E., 1996, *MNRAS*, 280, L37  
 Baugh C.M., Gaztañaga E., Efstathiou G., 1995, *MNRAS*, 274, 1049  
 Bernardeau F., 1992, *ApJ*, 392, 1  
 Bernardeau F., 1994a, *A&A*, 291, 697 (B94)  
 Bernardeau F., 1994b, *ApJ*, 433, 1  
 Bernardeau F., 1995, *A&A*, 301, 309  
 Bouchet F.R., Schaeffer R., Davis M., 1991, *ApJ*, 383, 19 (BSD)  
 Bouchet F.R., Hernquist L., 1992, *ApJ*, 400, 25 (BH)  
 Bouchet F.R., Juszkiewicz R., Colombi S., Pellat R., 1992, *ApJ*, 394, L5  
 Bouchet F.R., Strauss M.A., Davis M., Fisher K.B., Yahil A., Huchra J.P., 1993, *ApJ*, 417, 36  
 Bouchet F.R., Colombi S., Hivon E., Juszkiewicz R., 1995, *A&A*, 296, 575  
 Coles P., Jones B., 1991, *MNRAS*, 248, 1  
 Colombi S., Bouchet F.R., Schaeffer R., 1994, *A&A*, 281, 301 (CBSI)  
 Colombi S., Bouchet F.R., Schaeffer R., 1995, *ApJS*, 96, 401 (CBSII)  
 Colombi S., Bouchet F.R., Hernquist L., 1996, *ApJ*, 465, 14 (CBH)  
 Davis M., Efstathiou G., 1988, in *Large Scale Motions in the Universe*, ed. V.C. Rubin & G.V. Coyne (Princeton: Princeton Univ. Press), p. 256  
 Davis M., Peebles P.J.E., 1977, *ApJS*, 34, 425  
 Efstathiou G., Frenk C.S., White S.D.M., Davis M., 1988, *MNRAS*, 235, 715  
 Frenk C.S., White S.D.M., Efstathiou G., Davis M., 1990, *ApJ*, 351, 10  
 Fry J.N., 1984, *ApJ*, 277, L5  
 Fry J.N., Gaztañaga E., 1993, *ApJ*, 413, 447  
 Fry J.N., Melott A.L., Shandarin S.F., 1993, *ApJ*, 412, 504  
 Gaztañaga E., 1992, *ApJ*, 398, L17  
 Gaztañaga E., 1994, *MNRAS*, 286, 913  
 Gaztañaga E., Baugh C.M., 1995, *MNRAS*, 273, L1  
 Hamilton A.J.S., 1988, *ApJ*, 332, 67  
 Hamilton A.J.S., Kumar P., Lu E., Matthews A., 1991, *ApJ*, 374, L1  
 Hernquist L., Bouchet F.R., Suto Y., 1991, *ApJS*, 75, 231  
 Hivon E., Bouchet F.R., Colombi S., Juszkiewicz R., 1995, *A&A*, 298, 643  
 Jain B., 1996, preprint (astro-ph/9605192)  
 Jain B., Mo H.J., White S.D.M., 1995, *MNRAS*, 276, L25  
 Juszkiewicz R., Bouchet F.R., 1992, *Proceedings of the Second DAEC meeting*, Meudon, France, ed. G. Mamon & D. Gerbal  
 Juszkiewicz R., Bouchet F.R., Colombi S., 1993, *ApJ*, 412, L9  
 Juszkiewicz R., Weinberg D.H., Amsterdamski P., Chodorowski M., Bouchet F.R., 1995, *ApJ*, 442, 39  
 Lokas E.L., Juszkiewicz R., Weinberg D.H., Bouchet F.R., 1995a, *MNRAS*, 274, 730  
 Lokas E.L., Juszkiewicz R., Bouchet F.R., Hivon E., 1995b, *CAMK preprint 299/95* (astro-ph/9508032)  
 Martel H., Freudling, W., 1991, *ApJ*, 371, 1  
 Matsubara, T., Suto Y., 1994, *ApJ*, 420, 497  
 Maurogordato S., Schaeffer R., da Costa L.N., 1992, *ApJ*, 390, 17  
 Peacock J.A., Dodds S.J., 1994, *MNRAS*, 267, 1020

- Peebles P.J.E., 1980, *The Large Scale Structure of the Universe*  
(Princeton University Press, Princeton, N.Y., U.S.A.)  
Soccimarro R., 1996, Ph.D. thesis, The University of Chicago  
Soccimarro R., Frieman J.A., 1996, *ApJS*, 105, 37  
Szapudi I., Colombi S., 1996, *ApJ*, 470, 131  
Szapudi I., Meiksin A., Nichol R., 1996, *ApJ*, in press  
Szapudi I., Szalay A., Boschán P., 1992, *ApJ*, 390, 350  
White S.D.M., 1994, *Les Houches Lectures*, astro-ph/9410043